IOPscience iopscience.iop.org

Home Search Collections Journals About Contact us My IOPscience

Calculation of the complex bulk and surface-state band structure using the multislice matrix method

This article has been downloaded from IOPscience. Please scroll down to see the full text article.

1992 J. Phys.: Condens. Matter 4 8461

(http://iopscience.iop.org/0953-8984/4/44/008)

View the table of contents for this issue, or go to the journal homepage for more

Download details:
IP Address: 171.66.16.96
The article was downloaded on 11/05/2010 at 00:44

Please note that terms and conditions apply.

J. Phys.: Condens. Matter 4 (1992) 8461–8476. Printed in the UK

Calculation of the complex bulk and surface-state band structure using the multislice matrix method

C Stampfl†, K Kambe†, J D Riley‡ and D F Lynch§

† Fritz-Haber-Institut der Max-Planck-Gesellschaft, Faradayweg 4-6, 1000 Berlin 33, Germany

‡ Department of Physics, La Trobe University, Bundoora 3083, Australia

§ CSIRO Division of Materials Science and Technology, Clayton 3168, Australia

Received 14 May 1992, in final form 26 June 1992

Abstract. It is shown that the complex bulk band structure and the surface-state/resonance dispersions can be obtained using a dynamical scattering multislice matrix method previously developed for the calculation of LEED (low-energy electron diffraction), despite existing opinions that certain formalisms using the multislice method may be numerically unstable. Calculations have been performed for the free-electron-like metal magnesium and the semiconductor gallium arsenide as the first step of the calculation of photoemission intensity profiles from these materials. The obtained real and complex band structures, as well as the surface-state/resonance dispersions, have been compared to the results of other calculations and were found to show good agreement. In addition, an interesting behaviour of the wavefunction in the vicinity of certain projected bulk band edges was observed; it is seemingly related to a kind of 'beating' of the Bloch waves composing the wavefunction.

1. Introduction

This paper presents a method of calculation of the complex bulk band structure and surface-state/resonance dispersions of a crystal and is applied to the free-electron-like metal magnesium and the semiconductor gallium arsenide. The method uses a numerical scheme originally written to calculate low-energy electron diffraction (LEED) intensities [1,2]. The LEED scheme combines the multislice method of Cowley and Moodie [3] with the semi-reciprocal supermatrix method of Tournarie [4]. This numerical scheme has also been successfully used to calculate current image diffraction (CID) patterns [5] and has been modified to perform calculations of convergent beam reflection high-energy electron diffraction (CBRHEED) intensities [6].

Having obtained the LEED states and band structures they will be used in a one-step calculation of photoemission intensities. The final states are obtained as time-reversed LEED states, and the band structure states are used to calculate the initial-state wavefunctions in the valence band energy region. This will be the subject of a later paper. It is critical that the correct band structure is obtained, so the present results of real and complex band structures are compared with existing data obtained by other methods, so far as they are available. However, it should be kept in mind that, because pseudopotentials are used, the wavefunctions obtained will be the pseudowavefunctions.

0953-8984/92/448461+16$07.50 © 1992 IOP Publishing Ltd

Section 2 gives an outline of the LEED theory from which the band structure calculation was derived, while section 3 shows the results for the conventional and complex bulk band structures. Section 4 contains a description of how surface states and surface resonances can be obtained using the present method and shows the resulting surface-state/resonance dispersions for Mg and GaAs (in the $\bar{\Gamma}$–$\bar{X}'$ direction). In section 5 we present the conclusion. Contained in the appendix is an illustration of the unusual behaviour of the wavefunction found in the vicinity of certain kinds of projected bulk band edges. The convergence of the bulk band structure and wavefunctions are also discussed in the appendix.

2. Theory

It is useful to first describe the multislice matrix method for LEED, which is used to calculate the band structures. The method is given in detail in [2] and is outlined below.

By imposing Bloch periodicity, for given values of $(k_x, k_y) = k_\parallel$, the Schrödinger equation can be expressed in mixed representation, i.e. reciprocal space is used in the plane parallel to the surface (the x, y plane), but not in the z direction, perpendicular to the surface. The Schrödinger equation can then be written as a first-order matrix differential equation by using a supermatrix:

$$\frac{\mathrm{d}}{\mathrm{d}z}\begin{pmatrix} U(z) \\ U'(z) \end{pmatrix} = \begin{pmatrix} 0 & E \\ -M(z) & 0 \end{pmatrix}\begin{pmatrix} U(z) \\ U'(z) \end{pmatrix}.$$

Here $M(z)$ is a Hermitian matrix defining the scattering potential and E is the identity matrix. This equation can be written as

$$\mathrm{d}\Phi(z)/\mathrm{d}z = S(z)\Phi(z) \tag{1}$$

where

$$S(z) = \begin{pmatrix} 0 & E \\ -M(z) & 0 \end{pmatrix}$$

and $\Phi(z)$ is a supercolumn vector, of order two, containing the infinite column vectors $U(z)$ and $U'(z)$, which contain the wave amplitudes and their derivatives respectively.

If the crystal is split into a number of very thin slices with thickness Δz, S can be regarded as being independent of z in one slice. Thus, the solution to (1) for such a thin slice is

$$\Phi(\Delta z) = \exp(S\Delta z)\Phi(0).$$

The full solution is obtained by the product of solutions for the thin slices constituting the crystal. It is then possible to write

$$\begin{pmatrix} U(z) \\ U'(z) \end{pmatrix} = \Omega(z)\begin{pmatrix} U(0) \\ U'(0) \end{pmatrix} \tag{2}$$

where the matrix Ω is evaluated by a product of propagator operators for the thin slices of crystal:

$$\Omega(z) = \Omega_n(\Delta z_n) \ldots \Omega_2(\Delta z_2)\Omega_1(\Delta z_1).$$

For a slice

$$\Omega_n(\Delta z_n) = \exp(S_n \Delta z_n) = \exp\left[\begin{pmatrix} 0 & E \\ -M_n & 0 \end{pmatrix} \Delta z_n\right]. \tag{3}$$

Equation (2) gives a formalism for writing down an expression for the wavefunction $\psi(\boldsymbol{r})$ and its derivative $\psi'(\boldsymbol{r})$, at any point in the crystal, because the elements of U and U' (the amplitudes and their derivatives respectively) form the coefficients of the two-dimensional Fourier expansion of $\psi(\boldsymbol{r})$ and $\psi'(\boldsymbol{r})$.

2.1. *LEED intensities*

To obtain LEED intensities, boundary conditions are applied for a slab of crystal with thickness d, which is infinite in extent in the x and y directions, and surrounded by vacuum. The thickness d is chosen to be sufficiently thick so as to approximate the semi-infinite crystal. Continuity of the wavefunction and derivative are required at $z = 0$ and $z = d$. The resulting expression for the reflected wave amplitudes is given by

$$b = (\alpha + \beta)^{-1}(\alpha - \beta)a_0$$

where a_0 is a column vector containing the amplitude (equal to unity) of the incident wave and

$$\alpha = \mathrm{i}\Omega_{22}(d)K + K\Omega_{12}(d)K$$

and

$$\beta = \mathrm{i}K\Omega_{11}(d) - \Omega_{21}(d).$$

We write

$$\Omega(d) = \begin{pmatrix} \Omega_{11}(d) & \Omega_{12}(d) \\ \Omega_{21}(d) & \Omega_{22}(d) \end{pmatrix}$$

and

$$K = \begin{pmatrix} {}^{v}k_z^1 & \cdots & 0 \\ \vdots & \ddots & \vdots \\ 0 & \cdots & {}^{v}k_z^N \end{pmatrix}. \tag{4}$$

Here K is a diagonal matrix containing the normal components of the wavevectors of the waves in the vacuum. The LEED intensity is obtained by evaluating $b^{\dagger} b$.

It is necessary to truncate the matrix M_n (in equation (3)) and thus U and U' to a suitable size N. If N 'beams' (see [2]) are used, the matrices M_n and $\Omega(z)$ will be of dimensions $N \times N$ and $2N \times 2N$ respectively.

2.2. Bulk band structure

The bulk band structure is obtained from the secular equation for the Bloch function $U(z) = B(z)$ [7–10]. Using Bloch's theorem, it is required that

$$B(c) = \exp(ik_z c)B(0)$$

and from equation (2)

$$\Omega(c)B(0) = \exp(ik_z c)B(0) \tag{5}$$

where k_z is the component of the wavevector perpendicular to the surface and $\Omega(c)$ is the operator that translates a wavefunction from one plane to another equivalent plane one lattice spacing, c, away from the surface. (It is assumed here that the c axis lies perpendicular to the surface.) Therefore, from the eigenvalues $e^{ik_z c}$ of $\Omega(c)$, the complex bulk band structure $k_z(E)$ can be obtained for a given energy and $k_{\parallel}$.

The $2N$ eigenvectors of equation (5) contain the Bloch wave amplitudes and derivatives (evaluated at $z = 0$). With the use of equation (2) it is then possible to find the Bloch wave amplitudes (and their derivatives) at any point in the crystal. Bloch waves can be 'propagating' or 'evanescent' according to whether k_z is real or imaginary for real energy. In the presence of absorption (i.e. the imaginary part of the energy), N of the Bloch waves increase into the crystal with z, and N of them decrease with increasing z. The number of beams, N, in the calculation for the band structure differ depending on the particular crystal being studied. For complex structures with strong bonding between atoms a large value of N is required, while for free-electron-like materials fewer are needed (see below).

It should be noted that there exists the opinion that certain formalisms using the multislice method are numerically unstable when many evanescent waves are included [11, 12]. Several approaches have been taken to overcome this problem; for example, Zhao *et al* [12] use an embedding method evaluating only the reflection (R) matrices, while Maksym [13] has introduced a stabilization procedure based on the layer-doubling method of LEED, and Meyer-Ehmsen [14] has overcome this difficulty by calculating the reflectivity matrix of a perfect crystal directly from a set of non-linear first-order differential equations. Recently Ichimiya [15] has demonstrated the stability and convergence of his calculation method for obtaining RHEED intensities [16] using the multislice formalism. In the present calculation the problem of instabilities is not so acute, because pseudopotentials are used (see below) and for evaluating the Bloch waves only one lattice period is needed. Also, if a surface barrier is included, the potential distribution is generally a smooth slowly varying function, and therefore not as problematic as in the bulk region. A new method of avoiding the divergence caused by the instability is described briefly in the appendix. In any case, the stability and convergence of the present results have been checked everywhere. A few examples are given in the appendix. Ultimately the agreement with other band structure calculations can give us confidence that the calculations are sound.

2.3. The potential

It is reasonable to use a pseudopotential when calculating the properties of conduction/valence band electrons. A local pseudopotential must be used in the z direction because it is assumed in our calculation scheme that the wavefunction

$\psi(z)$, for values of z ahead of the point at which the evaluation is being carried out, is not known [7].

The potential used for calculating the band structure of magnesium was constructed using the tabulated local pseudopotential form factors given by Harrison [17] derived from the model pseudopotential of Heine and Abarenkov, which is an extension of the quantum defect model. For the GaAs band structure shown in figure 2, the crystal potential was constructed using the local pseudopotential form factors given by Cohen and Bergstresser [18]. An analytic form of the form factors (local pseudopotential) has been given by Humphreys and Srivastava [19] based on the empirical pseudopotential method, which makes it possible to find the form factor for any desired reciprocal lattice vector. These form factors were used in calculation of the band structures shown in figures 4, 5 and 7.

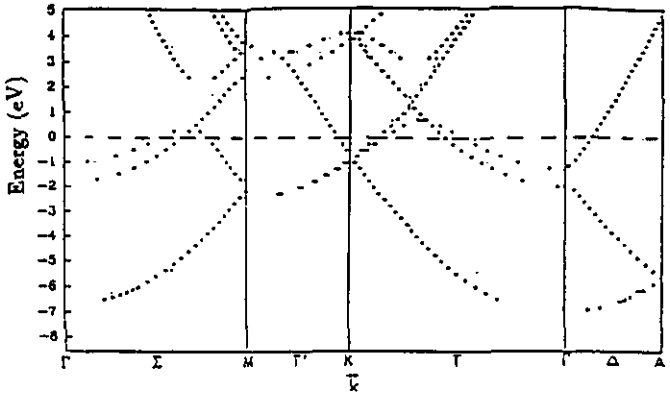

Figure 1. The band structure of magnesium calculated by the multislice matrix method using a pseudopotential derived from the local pseudopotential form factors given by Harrison [17].

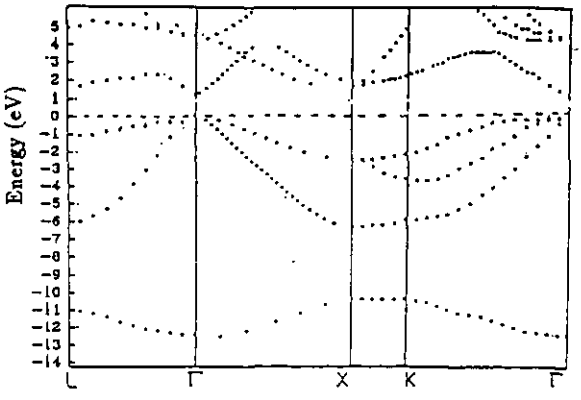

Figure 2. The band structure of GaAs calculated by the multislice matrix method using a pseudopotential calculated from the local pseudopotential form factors given by Cohen and Bergstresser [18].

In the multislice method it is easy to include an arbitrarily shaped surface barrier into the problem using various models. In the present work, however, a simple step barrier formed by sharply cutting off the three-dimensionally periodic bulk potential was used.

3. Results: bulk band structure

3.1. Conventional (real) band structure

3.1.1. Magnesium. For Mg the size of the supermatrix was 14 × 14 for the Γ–A direction, 10 × 10 for the Γ–M direction and 34 × 34 for the Γ–K–M direction. The number of slices used for the repeating cell, for both the Mg and GaAs calculation, was 16.

Table 1. Comparison of the energy gaps in the magnesium band structure. All entries are measured in eV.

Critical points	Present work	Ref. [26]	Ref. [24]	Ref. [27]	Ref. [25]		Ref. [28]
					APW(a)	APW(b)	
$\Gamma_4^- - \Gamma_3^+$	0.6	0.4	0.46	1.36	0.46	0.71	1.41
$M_2^- - M_1^+$	0.1		0.027	0.57	0.136	0.24	0.63
$K_5 - K_1$	0.1	0.2	0.027	0.73	0.19	0.35	0.57

The conventional band structure for magnesium calculated using this scheme is shown in figure 1. In table 1 some energy gaps of the present Mg band structure are compared with previous calculations (the last four columns were taken from the paper by Taut *et al* [24], being converted into eV for comparison). The method of calculation used by Blaha *et al* [26] is a full-potential linearized augmented plane wave (LAPW) method within a scalar relativistic description and assuming a local density approximation. Their results may be regarded as the most reliable among the available data. The band-gap values given for that of Blaha *et al* [26] may be slightly inaccurately reproduced because they were obtained from the figures shown in the paper by Blaha *et al* [26]. One finds overall a good agreement between the present and previously obtained band structures, the difference lying in our choice of the simplified pseudopotential of Harrison [17].

3.1.2. Gallium arsenide. In the plot shown in figure 2 it can be seen by comparing with figure 5 of Cohen and Bergstresser [18] that the present results agree very closely, as they should do because the same pseudopotentials were used. The supermatrix used in the calculation was of dimension 74 × 74.

In table 2 some critical points of the present GaAs band structure are compared with previous calculations. The third column in this table was given in the paper by Giovanni and Christensen [29]. It is a linear muffin-tin orbital calculation by Jarlborg and Freeman [30] and is in good agreement with the present calculation, to within 0.2 eV, except at the conduction band critical points X_1 and X_3, where the difference is 0.5 and 0.4 eV respectively. The results may also be compared to those by Tang [31], shown in the last column of the table. Tang treats the local pseudopotential Hamiltonian in the spatial representation by the tight-binding theory. Again the agreement is quite good, the critical values agreeing to within 0.3 eV except at the Γ_1 point, where the difference is 0.5 eV.

Table 2. Critical points of the GaAs band structure. All energies are measured in eV.

Critical points	Present work	Ref. [30]	Ref. [31]
Γ_1	−12.1	−12.3	−12.59
Γ_{15}	0.0	0.0	0.0
Γ_1	1.2	1.1	1.42
Γ_{15}	4.4	4.5	4.42
X_1	−10.2	−10.42	−10.55
X_3	−6.2	−6.20	−5.95
X_5	−2.4	−2.43	−2.18
X_1	1.6	2.07	1.87
X_3	1.9	2.31	2.12
L_1	−10.8	−11.06	−11.13
L_1	−6.0	−6.09	−6.27
L_3	−1.0	−1.02	−0.72
L_1	1.5	1.55	1.54
L_3	4.9	4.91	5.17

3.2. Complex band structure

When calculating the band structure for an infinite crystal the imaginary part of E is put equal to zero, leading to 'real lines' [32] in the complex band structure. In the calculation of photoemission intensities we need complex band structures obtained for complex energies. For energies above the vacuum level, the imaginary part of the energy represents the 'absorption' of a LEED electron (or the lifetime of a photoelectron in its final state), while for energies below the Fermi level the presence of such an imaginary part can be thought of as describing the lifetime of a hole state, which results after photoexcitation.

Figures 3 and 4(a) show three-dimensional complex band structures for Mg and GaAs respectively, where the real energy is plotted as a function of the real and imaginary parts (k_r, k_i) of k_z. Figure 4(b) shows (for GaAs) in a three-dimensional complex band structure plot the typical effect that a small (0.05 eV) constant imaginary part of the energy produces on the complex band structures. We have found that the use of a small imaginary part of energy is a great help in understanding the complicated band structure of GaAs. Figures 5(a) and (b) show an alternative projected representation of the complex band structure of GaAs in the [110] and [100] directions, for real energies.

For Mg we have not found in the literature comparative results of complex band structure. The complex band structure has been obtained by Smith *et al* [33] for GaAs (along the [001] direction, $k_{\parallel} = 0$). They use a pseudopotential and employ a (damped) plane-wave basis set. Complex band structures of zinc-blende materials have also been obtained by Chang [34] using an empirical tight-binding formalism. The complex band structures of Chang, for GaAs in the [100] and [110] directions, do not show qualitative agreement with the present calculations in the topological form of the imaginary and complex bands. (See Chang's figures 4 and 16.) It is to be noted, however, that for energies greater than the valence band maximum, the conventional real band structure of Chang already shows a qualitative deviation from other results (such as those referenced in table 2 including the present results, and those of [33]). It is suggested that a comparison of complex band structures may be useful for deriving proper parameters in an empirical scheme like that of Chang.

The complex band structure obtained by Smith *et al* [33] for GaAs in the [100]

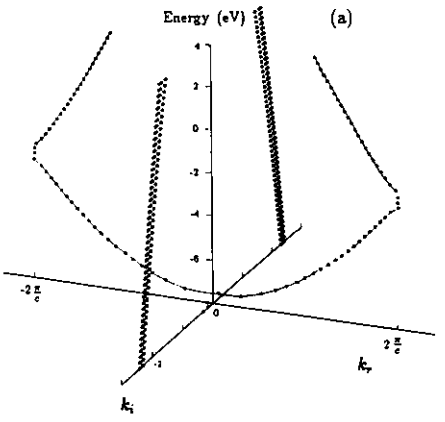

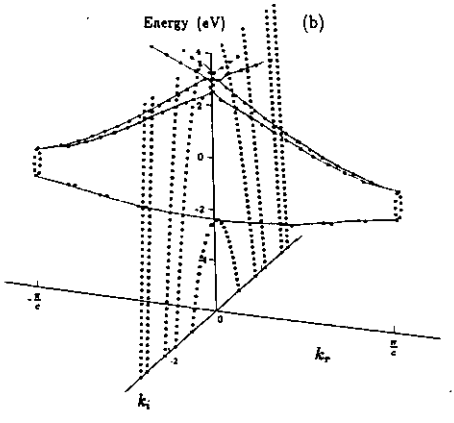

($k_{\|}$ = 1.7619Å^{-1})

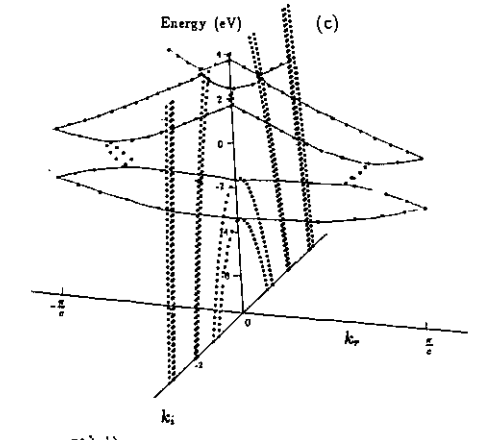

($k_{\|}$ = 1.0173Å^{-1})

Figure 3. Perspective representation of the complex band structure for Mg (*a*) for $k_{\|} = 0$, (*b*) for $k_{\|} = 1.7619\,\text{Å}^{-1}$ in the $[11\bar{2}0]$ direction and (*c*) for $k_{\|} = 1.0173\,\text{Å}^{-1}$ in the $[11\bar{1}0]$ direction (see figure 6). The circles connected by full curves show points on the real plane (k_i and k_r are in units of Å^{-1}). (Note that the imaginary loops at the two ends of (*b*) are different.)

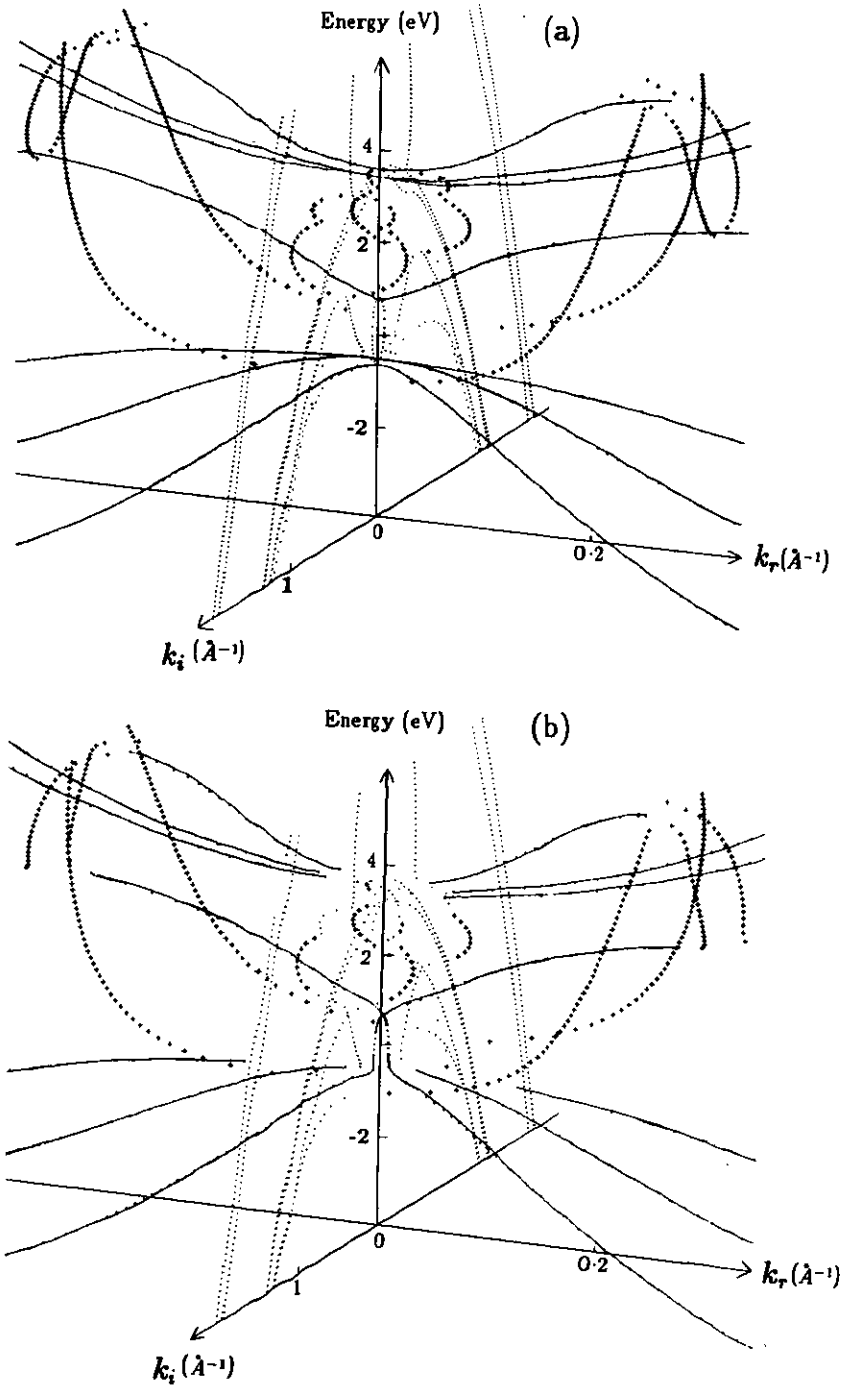

Figure 4. Perspective representation of the complex band structure for (*a*) an infinite crystal of GaAs in the Γ–K–X direction. The full curves show points lying on the real plane, i.e. the conventional band structure. (k_i and k_r are in units of Å^{-1}.) (*b*) Same as (*a*), except it is obtained with the imaginary part of the energy equal to 0.05 eV.

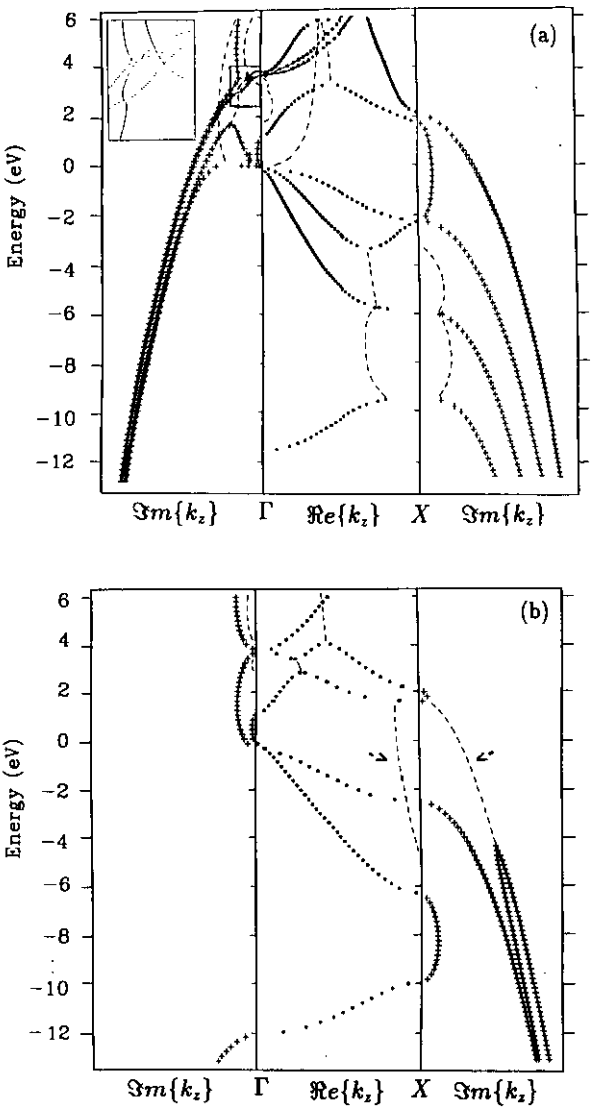

Figure 5. Usual projected representation. (*a*) The complex band structure of GaAs along the [110] direction where the band structure enclosed in the small rectangle has been enlarged for clarity, and (*b*) the complex band structure of GaAs along the [001] direction. In both cases the crosses correspond to imaginary bands, full circles to real bands and the pairs of broken curves to complex bands.

direction shows better agreement with the present results (figure 5(*b*)) than does the complex band structures obtained by Chang. However, on comparing figure 2 of [33] with figure 5(*b*) of the present paper, one difference is seen. The form of the complex band indicated with an arrow in figure 5(*b*) is different to the corresponding band shown in figure 2 of [33]. For the moment it is not clear whether the difference comes from the different choice of the method or from the model potential. In any case, our result for GaAs indicates that this complex band belongs to those 'novel topological structures' of Chang, as shown in his figure 23.

4. Surface-state/resonance band structure

As mentioned in the introduction, the present multislice method will form the basis for a one-step calculation of photoemission intensities. The final states being taken as the time-reversed LEED states and the initial states will be formed from a linear combination of Bloch waves obtained in the calculation of the complex band structure as the eigenvectors in (5). For details we refer to [35]. The initial state can be written as

$$U^m(z) = B_i^+(z)c^m + b_i^{m-}(z)c^{m-} \tag{6}$$

where c^m is a column vector containing the N coefficients of the Bloch waves $B_i^+(z)$ travelling or evanescent into the crystal, and the superscript m corresponds to the mth Bloch wave $b_i^{m-}(z)$ propagating towards the surface from the bulk. By matching the waves and derivatives across the vacuum/crystal boundary ($z = 0$), neglecting the surface-barrier/over-layer region for simplicity, the equation below is obtained, from which the ratio c^m/c^{m-} can be determined:

$$(B_i'^+(0) + \mathrm{i}KB_i^+(0))c^m = -(b_i'^{m-}(0) + \mathrm{i}Kb_i^{m-}(0))c^{m-} \tag{7}$$

where $b_i'^{m-}$ and $B_i'^+$ represent the derivatives, and K is a diagonal matrix containing the normal components of the wavevectors of the waves in vacuum (see equation (4)); c^{m-} is determined by normalization of the initial-state wavefunction. This equation can be easily modified to include a surface-barrier/over-layer.

The surface-state/resonance band structure using the present method can be obtained by considering the condition that there is a solution to equation (7) when there is no incident wave ($c^{m-} = 0$). That is, surface states/resonances exist at the zeros/nearly zeros of the determinant of matrix $(B_i'^+ + \mathrm{i}KB_i^+)$, or more conveniently, of the Hermitian matrix

$$\det[(B_i'^+ + \mathrm{i}KB_i^+)^\dagger(B_i'^+ + \mathrm{i}KB_i^+)] = 0/\approx 0 \tag{8}$$

where the calculation is made without the imaginary lifetime parameter. We have found that equation (8) does not always correspond to a surface-state/resonance, particularly at band edges and saddle points of imaginary bands (e.g. inside the fundamental band gap of GaAs). In these cases equation (8) shows a sharp minimum, whereas for a surface-state/resonance a parabolic form of the minimum appears. It is necessary to plot the wavefunction as a function of distance into the crystal and note whether it has the form typical of a surface state/resonance (see figure A2).

The surface-state/resonance band structure has been calculated by this method for Mg and GaAs ($\bar{\Gamma}$–$\bar{X}'$ direction) using the step barriers and the terminated bulk lattice structures. The result for Mg is shown in figure 6. The open circles represent the bulk band edges and the position of the surface-states/resonances by smaller full circles. The surface electronic structure of Mg(0001) has been calculated by Chulkov *et al* [20] using the slab method (a ten-layer film was used). On comparing figure 6 with figure 10 of [20], it can be seen that the band structures obtained by the two methods are very similar. However, in the present calculation two additional surface resonance bands were obtained, which are situated near the $\bar{M}$ point at approximately 2.2 eV and near the $\bar{K}$ point at approximately 1.5 eV (both are indicated by a broken

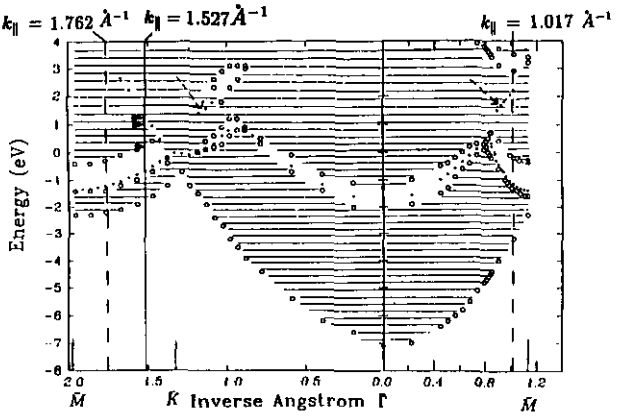

Figure 6. The surface-state/resonance band structure of Mg (0001) obtained using the present method. The small dots denote the position of the surface-states/resonances and the open circles denote projected bulk band edges. Perpendicular broken lines may be compared to figures 3(*b*), (*c*), and the perpendicular line with tags to figure A2.

arrow). When using the slab method the classification of a surface resonance may be somewhat difficult, for if the slab is taken to be too thin it may be difficult to detect a slowly decaying surface-resonance wave. This may partly explain the absence in [20] of the extra resonances observed in the present work.

In the present study a rather interesting behaviour of the wavefunction was observed at the positions of a minimum of expression (8) occurring at band edges as mentioned above; see, for example, figure A2(*a*), which is different to that of a surface state or resonance as shown in figure A2(*c*) and different to that of an arbitrary initial state such as that shown in figure A2(*b*). It is possible that there exists a kind of 'beating' of the Bloch waves which compose the wavefunction at that energy. This idea will be investigated further in a later paper.

The surface-state/resonance dispersions have also been calculated for GaAs (110) in the $\bar{\Gamma}$–$\bar{X}'$ direction using the multislice method. The results are shown in figure 7. They were obtained assuming an unrelaxed (1×1) surface structure, i.e. the terminated bulk structure. The results obtained using the present method are shown as crosses, the bulk band edges are represented by open circles and the region of the projected bulk bands is shown as the hashed area. The present results can be compared with the earlier calculations by Schmeits *et al* [36] (shown as full circles in figure 7) and Ferraz *et al* [37] (shown as the broken lines in figure 7), who use a tight-binding scattering-theoretical method and a self-consistent pseudopotential method respectively, and also assume an unrelaxed (1×1) surface. In all of the calculations two surface states are present throughout the $\bar{\Gamma}$–$\bar{X}'$ section of the Brillouin zone in the fundamental gap occurring in the energy region of approximately 0 to 1.5 eV. The position of these two bands in each calculation are slightly different, however they

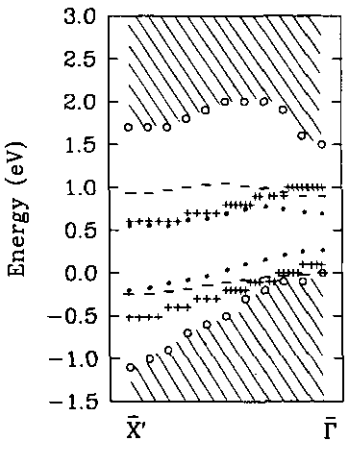

Figure 7. The surface-state/resonance band structure of GaAs (110) in the $\bar{\Gamma}$–$\bar{X}'$ direction, assuming an unrelaxed surface. The crosses show the surface states obtained using the present multislice method, the full circles are the results of Schmeits *et al* [36], and the broken lines are the surface states obtained by Ferraz *et al* [37].

are within 0.5 eV of each other.

It is well known that the relaxation effects for GaAs (110) are significant [21–23] and have a strong influence on the surface state/resonance band structure; therefore for calculations particularly concerned with surface states/resonances, an accurate potential must be used in the surface region [38].

5. Conclusion

It has been demonstrated that the method presented, based on a multislice formalism for LEED, can be used successfully to calculate the conventional and complex bulk band structure and the surface-state/resonance band structure of solids. It has been applied to Mg and GaAs, where good agreement with previous results were obtained.

In addition, an interesting behaviour of the wavefunction in the vicinity of a particular kind of projected bulk band edge was observed; it satisfies, incidentally, the same existence conditions of surface resonances and is seemingly related to a kind of 'beating' of the Bloch waves composing the wavefunction.

It is noticed that the present multislice method may be a useful alternative to the various methods of obtaining surface and interface electronic states such as those discussed by Smith *et al* [33], for example in analysing semiconductor heterojunctions.

Acknowledgments

C Stampfl would like to thank both the Education Department of Australia for a Commonwealth Postgraduate Award and the Deutscher Akademischer Austauschdienst (DAAD) for a research grant, and Professor M Scheffler for use of the facilities at the Fritz-Haber-Institut where part of the present work was carried out. Dr R Leckey is also thanked for helpful discussions.

Appendix.

The convergence of the band structure (wavevector k_z for $k_{\parallel} = 0$) as a function of basis set size (number of beams) is illustrated by a few examples, as shown

in figure A1(a) for GaAs (110) for the energies indicated (in eV and relative to the valence band maximum obtained for 29 beams). The results indicate that the calculation of band structures is sufficiently stable in the present range of parameters.

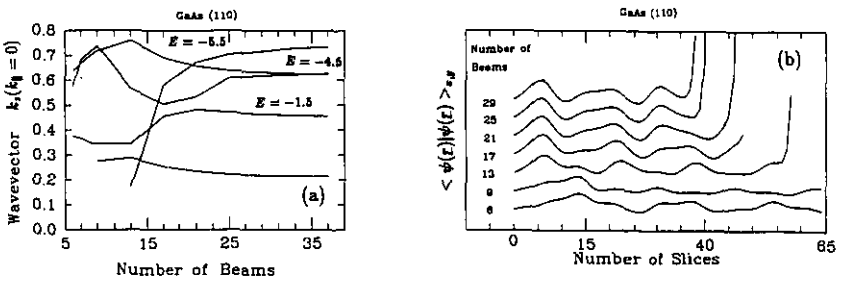

Figure A1. (a) GaAs (110). The perpendicular component of the wavevector k_z ($k_\parallel = 0$) (Å^{-1}) plotted as a function of the number of beams N for the three energies indicated (in eV and relative to the valence band maximum for 29 beams). The slice thickness was 0.250 Å and there were 16 slices per period. (b) GaAs (110). A plot of the x, y average of $\psi(r)$ squared, $\langle\psi(r)|\psi(r)\rangle_{x,y}$, as a function of the number of slices, obtained with an energy of −4.5 eV (relative to the valence band maximum for 29 beams) and using the number of beams N indicated ($k_\parallel = 0$).

Figure A1(b) shows a few examples for GaAs (110) of the variation of the x, y average squared of $\psi(r)$, $\langle\psi(r)|\psi(r)\rangle_{x,y}$, derived from equations (5) and (6) without an imaginary potential, with both slice number and the number of beams. The position of $z = 0$ is the vacuum/bulk crystal boundary. One finds that the curves converge with an increasing number of beams, but an ultimate divergence at a certain depth occurs when the function is evaluated beginning at the vacuum side, and is apparently due to the effect of increasing evanescent waves introduced by a numerical error. The divergence occurs earlier for a larger number of beams due to the effect of more strongly increasing evanescent waves. We note, however, that nothing serious happens within the first period (16 layers). The results remain practically the same for the calculations using 32 layers per period.

We have found that the solution in further depths can be evaluated without divergence by using equation (6). The multislice calculation is done only in the first period ('cell') of the bulk and, when necessary, the surface barrier. The values of Bloch waves $B_i^+(z)$ and $b_i^{m-}(z)$ appearing in (6) are evaluated inside the first cell and stored. The values of $U^m(z)$ for succeeding cells are constructed by multiplying each of the Bloch waves by its proper exponential factor according to (5), i.e. $\exp[ik_z^n c(q-1)]$ for the nth Bloch wave in the qth cell. The curves shown in figure A2 are derived using this new method.

In figures A2(a), (b) and (c) are shown plots of $\langle\psi(r)|\psi(r)\rangle_{x,y}$ for Mg(0001) as a function of slice number for three initial states, each with $k_\parallel = 1.527$ Å in the $\bar{\Gamma}$–$\bar{K}$–$\bar{M}$ (or [11$\bar{2}$0] direction (figure 6).) The first, present just at the band edge at an energy of 0.21 eV, displays an unusual behaviour. It appears that some kind of enhancement is occurring, perhaps due to 'beating' of the Bloch waves composing the initial states. The second plot represents an arbitrary example of the usual type of variation of $\langle\psi(r)|\psi(r)\rangle_{x,y}$, in this case at an energy of 1.0 eV. The third shows

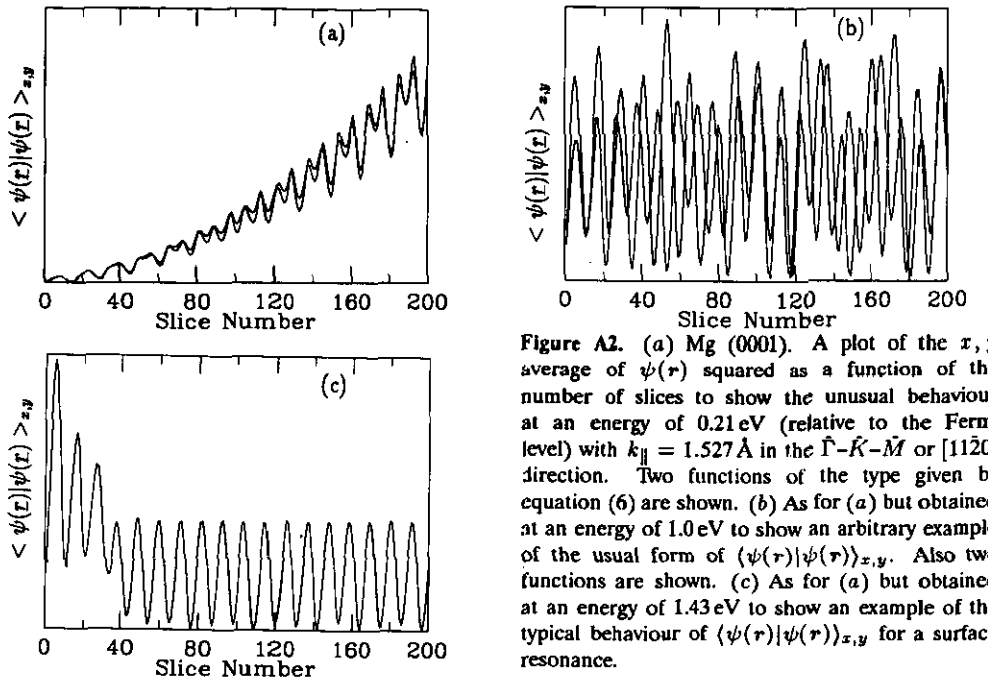

Figure A2. (*a*) Mg (0001). A plot of the x, y average of $\psi(r)$ squared as a function of the number of slices to show the unusual behaviour at an energy of 0.21 eV (relative to the Fermi level) with $k_{\parallel} = 1.527\,\text{Å}$ in the $\bar{\Gamma}$–$\bar{K}$–$\bar{M}$ or [11$\bar{2}$0] direction. Two functions of the type given by equation (6) are shown. (*b*) As for (*a*) but obtained at an energy of 1.0 eV to show an arbitrary example of the usual form of $\langle\psi(r)|\psi(r)\rangle_{x,y}$. Also two functions are shown. (*c*) As for (*a*) but obtained at an energy of 1.43 eV to show an example of the typical behaviour of $\langle\psi(r)|\psi(r)\rangle_{x,y}$ for a surface resonance.

the typical behaviour of $\langle\psi(r)|\psi(r)\rangle_{x,y}$ for a surface-state resonance (at an energy 1.43 eV) where the enhancement of the wavefunction near the surface can be seen.

References

[1] Lynch D F and Moodie A F 1972 *Surf. Sci.* **32** 422
[2] Lynch D F and Smith A E 1983 *Phys. Status Solidi (b)* **119** 355
[3] Cowley J M and Moodie A F 1957 *Acta Crystallogr.* **10** 609
[4] Tournarie M 1962 *J. Phys. Soc. Japan* **17** 98
[5] Smith A E and Lynch D F 1986 *Surf. Sci.* **184** 189
[6] Smith A E 1987 *J. Vac. Sci. Tech.* **5** 1262
[7] Jepsen D W, Marcus P M and Jona F 1971 *Phys. Rev. Lett.* **26** 1365
[8] Marcus P M and Jepsen D W 1968 *Phys. Rev. Lett.* **20** 925
[9] Pendry J B 1974 *Low Energy Electron Diffraction: The Theory and its Application to Determination of Surface Structure* (London: Academic)
[10] Pendry J B and F Forstmann 1969 *J. Phys. C: Solid State Phys.* **3** 59
[11] Wachutka G 1986 *Phys. Rev.* B **34** 8512
[12] Zhao T C, Poon H C and Tong S Y 1988 *Phys. Rev.* B **38** 1172
[13] Maksym P A 1988 *RHEED and Reflection Electron Imaging of Surfaces* ed P K Larsen and P J Dobson (New York: Plenum)
[14] Meyer-Ehmsen G 1989 *Surf. Sci.* **219** 177
[15] Ichimiya A 1990 *Surf. Sci.* **235** 75
[16] Ichimiya A 1983 *Japan. J. Appl. Phys.* **22** 176
[17] Harrison W A 1966 *Pseudopotentials in the Theory of Metals* (New York: Benjamin)
[18] Cohen M L and Bergstresser T K 1966 *Phys. Rev.* B **141** 789
[19] Humphreys T P and Srivistava G P 1982 *Phys. Status Solidi (b)* **112** 581
[20] Chulkov E V, Silkin V M and Shirykalov E N 1987 *Surf. Sci.* **188** 287
[21] Chiang T, Ludeke R, Aona M and Landgren G 1983 *Phys. Rev.* B **27** 4770
[22] Duke C B and Paton A 1985 *Surf. Sci.* **164** L797
[23] Mailhiot C and Duke C B 1985 *Phys. Rev.* B **31** 2213

[24] Taut M and Ziesche P 1976 *Phys. Status Solidi (b)* **78** 169
[25] Dimmock J 1971 *Sol. State Phys.* **26** 103
[26] Blaha P and Schwarz K 1987 *Phys. Rev.* B **38** 9368
[27] Chatterjee S and Parsathi S 1975 *J. Phys. F: Met. Phys.* **5** 2089
[28] Falicov L 1962 *Phil. Trans. R. Soc.* A **225** 55
[29] Giovanni B B and Christensen N E 1985 *Phys. Rev.* B **31** 879
[30] Jarlborg T and Freeman A T 1979 *Phys. Lett.* **74A** 349
[31] Tang D S 1988 *Phys. Rev.* B **38** 12487
[32] Heine V 1964 *Surf. Sci.* **2** 1
[33] Smith D L and Mailhiot C 1990 *Rev. Mod. Phys.* **62** 173
[34] Chang Y 1982 *Phys. Rev.* B **25** 605
[35] Stampfl C M, Kambe K, Riley J D and Lynch D F 1992 *to be published*
[36] Schmeits M, Mazur A and Pollmann J 1983 *Phys. Rev.* B **27** 5012
[37] Ferraz A C and Srivistava 1987 *Surf. Sci.* **182** 161
[38] Hebenstreit J, Heinemann M and Scheffler M 1992 *to be published*